Nanofabrication (2022) 7
https://doi.org/10.37819/nanofab.007.227

RESEARCH ARTICLE

Cytotoxicity of curcumin-loaded magnetic nanoparticles against normal and cancer cells as a breast cancer drug delivery system

Ali Mollaie Ghanat Alnooj[1,2], Melika Ghobadi[1], Mohammad Mousavi-Khattat[3], Dina Zohrabi[1], Mohammad Sekhavati[2], Ali Zarrabi[4]*

[1]*Department of Biology, Faculty of Sciences, Nour Danesh Institute of Higher Education, Meymeh, Isfahan, Iran.*
[2]*Department of Aerobic Bacterial Research and Vaccine Production, Razi Vaccine and Serum Research Institute, Agriculture Research, Education and Extention Organization (AREEO), Karaj, Iran.*
[3]*Department of Biotechnology, Faculty of Biological Science and Technology, University of Isfahan, Isfahan.*
[4]*Department of Biomedical Engineering, Faculty of Engineering and Natural Sciences, Istinye University, Istanbul 34396, Turkiye*
**Corresponding author email: ali.zarrabi@istinye.edu.tr*

ABSTRACT

Recently, therapeutic applications of modified magnetic nanoparticles have attracted the attention of many researchers. The reason is the ability to develop nano drugs as cancer treatment agents. For this purpose, these particles must have a tiny size, intrinsic magnetic properties, imaging effectiveness, the ability to target the drug, and high drug absorption. Although studies have been performed on the anti-cancer properties of curcumin/nanoparticles, no comprehensive research has been performed to evaluate its anti-cancer and the normal cell toxicity of this drug system for breast cancer treatment. This study designed a curcumin-loaded MNPs (MNPs@CUR) formulation to accomplish these unique features. Using the diffusion process, chemical precipitation was used to make MNPs, which were then loaded with curcumin (CUR). Transmission electron microscopy (TEM) was used to study the morphology and size of MNP-CUR. The fabricated MNPs had spherical shapes with an average length of 23.22 nm. The presence of curcumin on the surface of MNPs was approved using Fourier transform infrared (FTIR) analysis. The X-ray diffraction (XRD) diffractogram confirmed the face cubic center (fcc) character of MNPs. After 24 hours of incubation with 4t1 breast cancer cells, MNPs@CUR anticancer effects were evaluated. MNPs@CUR displayed a concentration-dependent preference for applying anticancer effects on 4t1cells (IC_{50}=108 µg/ml). Separated *in vivo* anti-tumor studies of coated/naked nanoparticles and curcumin also demonstrated that MNPs@CUR eliminated tumor mass. The cytotoxicity and genotoxicity against normal peripheral blood mononuclear cells (PBMC) were also measured by 2,5-diphenyl-2H-tetrazolium bromide (MTT) electrophoresis DNA digestion methods respectively for MNPs@CUR and naked MNPs. Cytotoxicity was demonstrated at high concentrations of MNP@CUR (991 µg/ml), while naked nanoparticles showed approximately no toxicity and neither had genotoxicity.

ARTICLE HISTORY

Received: 02-07-2022
Revised: 15-09-2022
Accepted: 15-10-2022

KEYWORDS

Magnetic nanoparticles;
Curcumin;
Breast;
Cancer;
4t1;
Drug delivery

Introduction

Cancer is one of the leading causes of death worldwide (Brenner et al., 2020). Global statistics show that about 19.3 million new cases of cancer and approximately 10 million deaths due to cancer occurred in 2020 (Sung et al., 2021). Breast cancer is the most frequent cancer among women and is also one of the leading causes of mortality among them (Desreux, gynecology, & biology, 2018). Basal-like breast cancer accounts for about 15% of all reported breast cancer cases and has a poor prognosis. Most of these malignancies are triple-negative breast cancers because they do not overexpress the estrogen receptor, progesterone receptor, or human epidermal growth factor receptor 2. (P. Dutta et al., 2018; O'Meara et al., 2020; Wang et al., 2018). As a form of triple-negative breast cancer, 4t1cancer cells have a high rate of metastatic spread. Chemotherapy is an important treatment choice for triple-negative breast cancers. Still, it is often associated with a variety of side effects, including hair loss, fatigue, loss of appetite, nausea and vomiting, constipation or diarrhea, mouth sores, skin and nail changes, increased risk of developing infection (due to fewer white blood cells that help fight infection) (Abotaleb et al., 2018; George Kallivalappil & Kuttan, 2019; Palesh et al., 2018). Natural chemicals found in ordinary foods can be used to mitigate or eliminate the adverse effects of chemotherapy. Curcumin (CUR) is a natural diphenol obtained from the rhizomes of *Curcuma longa*. Because of its antioxidant, anti-inflammatory [4], antimutagenic, antibacterial [5,6], and anticancer characteristics, Curcuma longa has been traditionally utilized as a medical herb in Asian countries (Roychoudhury et al., 2021). According to research, curcumin may aid in the treatment of oxidative and inflammatory disorders, metabolic syndrome, arthritis, anxiety, and hyperlipidemia (Shah et al., 2022). it has several biological activities, including anticancer and chemoprevention (Patra et al., 2021). CUR could efficiently upregulate the expression of p53, p21, and p27 proteins and downregulate cyclin E, arresting the cancer cells in the G1 phase of the cell cycle (Ali & Smiley, 2018; Fratantonio et al., 2019). CUR also inhibits constitutive STAT3 (Signal transducer and activator of transcription 3) signaling and reduces cell viability and anchorage independence in breast cancer cells by inducing apoptosis (Khan et al., 2020). Moreover, it could change cell localization and phosphorylation, damage DNA, and alter BRCA1 (BReast CAncer gene 1), which is expressed in triple-negative breast cancer cells. (Guney Eskiler et al., 2020). CUR has also been shown to have synergistic antiproliferative effects when combined with other chemotherapeutic drugs or radiation (Abdallah, Helmy, Katary, & Ghoneim, 2018; Zoi et al., 2021). According to recent studies, CUR has a distinct function in cancer cells versus normal cells (Cianfruglia, Minnelli, Laudadio, Scirè, & Armeni, 2019). CUR, in particular, appears to have little effect on normal human cells. However, before CUR can be successfully utilized in a clinical context, difficulties like low water solubility, degradation in the physiological medium, and fast metabolism must be tackled (D'Angelo et al., 2021). Advanced drug delivery technologies could help accomplish these obstacles (D'Angelo et al., 2021). Recent studies have demonstrated that encasing or encapsulating CUR in nanocarriers including polymeric nanoparticles, nano-assemblies, and self-assemblies improves its localization and thereby induces cytotoxicity and death in cancer cells (Bai et al., 2020; Fu et al., 2021; Lee, Loo, Rohanizadeh, & C, 2019; Pan et al., 2020).

Magnetic nanoparticles have often found wide applications in medicine. These particles have been used in the manufacture of drug nanocarriers as contrast enhancers in magnetic resonance imaging as well as topical treatment with hyperthermia and a type of targeting called magnetic targeting (Nam et al., 2020; Yusefi, Shameli, & Jumaat, 2020). On the other hand, high aggregation of magnetic nanoparticles is a common problem. Opsonization begins with high aspect ratios and van der Waals powers, a significant challenge for medical applications. This problem can be solved by coating MNPs (Magnetic nanoparticles) with different stabilizing coatings, such as surfactants and synthetic/natural polymeric materials (Nam et al., 2020). Also, according to previous studies, some special polymers by coating around nanoparticles can improve the contrast in MRI imaging (Arsalani et al., 2019; Baki, Remmo, Löwa, Wiekhorst, & Bleul, 2021; Ostroverkhov et al., 2019). In general, nanotechnology has provided a platform for coating nanoparticles and solving the problems mentioned above.

As cancer nanotechnology advances, new clinical procedures such as nano theranostics, which uses tailored diagnostic treatment, are becoming

more common (Bakshi, Zakharchenko, Minko, Kolpashchikov, & Katz, 2019). The aim was to create a perfect magnetic nanoformulation with essential imaging and drug delivery features. In addition to drug delivery, other methods developed using magnetic nanoparticles include thermal light therapy, heat-responsive therapy, and visible/ luminescence / near-infrared / multifaceted imaging. (Bu et al., 2019; Sun et al., 2019; Wu et al., 2019). The biocompatibility, drug loading capacity, resistance in the biological environment, as well as high uptake of drugs by cancer cells all depends on the surface and the coating on it (Aguilera et al., 2019; Nosrati et al., 2018; Oroujeni, Kaboudin, Xia, Jönsson, & Ossipov, 2018). However, coated nanoparticles have a higher hydrodynamic diameter (250 nm) in aqueous conditions, limiting their usage as effective therapeutic carriers for medicinal applications.

In this study, the MNPs has constructed through the co-precipitation method and coated with curcumin as an anticancer agent to prevent cancer cell proliferation. The resulting particles were characterized by XRD, FTIR, VSM, and microscopic methods to prove the synthesis and coating of magnetic nanoparticles. The nanometer size of the particles used in this study can cause the particles to penetrate the cells and induce various anti-cancer mechanisms by the anticancer drug it is carrying. Also, due to the anti-cancer properties of curcumin, which is placed on magnetic nanoparticles, the effect of this herbal drug will apply with increased efficiency (Lopez-Barbosa et al., 2019). Also, because the behavior of nanoparticles due to metabolic pathways differs from the outside to the inside of the body, the tumor removal process was monitored in animals to ensure the therapeutic properties of the drug delivery system (Chenthamara et al., 2019). The final objective of this study was the analysis of the anti-cancer activity of synthesized coated nanoparticles against cancer cells and the cytotoxic activity against normal cells, and their DNA investigated simultaneously.

Materials and methods

Chemicals:

Iron (III) chloride ($FeCl_3$), iron (II) chloride ($FeCl_2 \cdot 4H_2O$), N, N Dimethylformamide 99.8%, curcumin, ethanol 96%, 3-(4, 5-dimethyl-2-thiazolyl)-2, 5-diphenyl- tetrazolium bromide (MTT), Trypsin, Phosphate buffered saline (PBS), Dimethyl sulfoxide (DMSO) 99.9% and sodium hydroxide (NaOH) were purchased from Sigma-Aldrich, Germany. 4t1 cells were kindly provided by the Razi vaccine and serum research institute, Karaj, Iran. RPMI (Roswell Park Memorial Institute) 1640 medium, Penicillin-Streptomycin antibiotics mixture, and fetal bovine serum (FBS) were supplied from Thermofisher, USA.

Preparation of magnetite (Fe_3O_4) nanoparticles:

Superparamagnetic iron oxide nanoparticles were prepared via the co-precipitation method using iron (III) chloride ($FeCl_3$) and iron (II) chloride ($FeCl_2 \cdot 4H_2O$) at a ratio of 2:1. Both iron precursors were dissolved in treated deionized water and allowed to mix for 80 min before heated up to reflux. When the solution temperature reached 80 °C, 10 milliliters of sodium hydroxide (NaOH) were added to the mixture. The complete reaction process was carried out under continuous nitrogen gas to provide an oxygen-free environment. The black precipitate was separated by centrifugation at 3,000 rpm for 30 min and washed with deionized water several times till reached to pH 7. To eliminate the residual water, the powders were dried overnight at 180°C. To increase the crystallinity of the produced NPs, the dried powders were calcined in an electrical vacuum furnace at 600 °C for 6 hours (Osorio Jaimes, 2020).

Stabilization and functionalization of nanoparticles (Fe_3O_4):

To stabilize and functionalize the prepared nanoparticles, 100 mL water, 0.080 g SDS powder was dissolved, vortexed, and left undisturbed until the foam transformed into a solution. It was warmed in a water bath for 20 minutes at 70°C, then centrifuged at 10,000 g, and the clear solution was collected and utilized. Meanwhile, 5 mL N, N dimethylformamide was used to wash 0.008 g of magnetically separated MNPs. The MNPs were separated using magnets and distributed in newly prepared 20 mL SDS, which was gently mixed for five minutes before being combined in a cyclo-rotator for three days (Justin, Samrot, Sahithya, Bhavya, & Saipriya, 2018).

Curcumin loading

2 mL N, N Dimethylformamide was used to dissolve 0.02 g curcumin powder. 400 µl of the curcumin mentioned above was added to the MNPs solution (0.008g in 20 ml deionized water) and stirred gently for 5 minutes. It was then placed in a rotator for 24 hours. After one day, the curcumin's magnetic nanoparticles were transferred to 2 ml microtubes. The mixture was shaken gently every three minutes to ensure that the temperature was evenly distributed. Magnetically separated curcumin-loaded particles were washed three times with distilled water and then placed in a freeze-dryer (Justin et al., 2018).

Analysis Methods:

The crystallographic structure of nanoparticles and elemental composition was analyzed via XRD (X-ray diffraction) (Rigaku D/Max IIIC, Cu-Kα radiation, Netherlands). Their size and shape were determined through microscopic characterizations by FESEM (field emission scanning electron microscopy) (JEOL JSM 6460LA) and TEM (transmission electron microscopy) (Philips: model CM 12, Netherlands) operated at 200 kV. For the calculation of particle size distribution, the program ImageJ was used for SEM and TEM images of nanoparticles and nanofibers. Surface nanoparticle composition was studied through FTIR (Fourier Transform Infrared Spectroscopy) (Perkin Elmer 5DX, USA). Finally, VSM (vibrating sample magnetometry) (Lake Shore 7303–9309, USA) was used to study the magnetic properties of the resulting nanoparticles.

***In vitro* cytotoxicity test:**

A standard cell proliferation assay was employed to assess *In vitro* cytotoxicity of naked MNPs, free curcumin, and MNPs @CUR against normal peripheral blood mononuclear cells (PBMC). For this experiment, healthy human volunteers' peripheral blood mononuclear cells were extracted using a normal density gradient centrifugation process (Gómez-Archila, Palomino-Schätzlein, Zapata-Builes, & Galeano, 2021). PBMC (1×105 cells/well) were cultured in RPMI-1640 media, treated with different concentrations of MNPs @CUR, the curcumin, and MNPs (31.25–1000 µg/ml), and then incubated for 24 hours at 37°C with 5% CO2. All samples were dissolved in PBS (Phosphate Buffer Saline) to avoid the effect of the solvent on the cells. Equivalent amounts of dimethyl sulfoxide (DMSO) in PBS were controls for this experiment (Hwang, Jeong, Jung, Nam, & Lim, 2021). In each well, the media was replaced after 24 hours with fresh media (100 µl) and 5mg/ml MTT reagent (20 µl). After incubation for 2 hours, the formazan crystals as a result of the transformation of MTT, were solubilized by DMSO in 5 minutes. Using a microplate reader (BioTek 800TS, USA), the absorbance of the color caused by the generation of solubilized crystals was quantified at 570 nm (Septisetyani, Santoso, Wisnuwardhani, & Prasetyaningrum, 2020). The amount of living cells in the culture is directly related to the absorption reading. The percentage of cell growth was calculated through equation 1. The experiments were repeated in triplicate, and the statistical analysis was done using Duncan's test (*p<0.05).

$$\% \text{ cell growth} = \frac{\text{treated cell absorption}}{\text{non-treated cell absorption}} \times 100 \qquad (1)$$

In vitro anticancer test:

In this study, we tested the anticancer effect of loaded curcumin-loaded MNPs on the 4t1cancer cell line as a model because it is highly tumorigenic and invasive (Nigjeh, Yeap, Nordin, Rahman, & Rosli, 2019). 4t1Cells were grown at 37 °C in RPMI supplemented with 10% FBS in a humidified environment containing 5% carbon dioxide. The cells were trypsinized once they reached 80 per cent confluence and transplanted to 96-well tissue cultivation plates with a density of 1 × 105 cells per well and incubated for 24 hours. After that, the medium was replaced with fresh medium containing (MNPs @CUR), free curcumin, and Fe_3O_4 at various concentrations (3.2–204.8 µg/ml) and incubated for 24 hours at 37°C with 5% CO2. After removing the sample solution and washing it with phosphate-buffered saline, MTT buffered saline solution (5 mg/mL) was added (pH 7.4). After the cells were incubated for 4 hours with treatment, 100 µl of DMSO was added to each well, and its absorbance was measured at 570 nm using a microplate reader (Stat Fax 3200 Microplate Reader, Awareness Technology, USA). The percentage of cell growth was calculated through the same formulae mentioned in the previous section. IC50% means the experiments were repeated in triplicate, and the statistical analysis was done using Duncan's

test (*p<0.05). For all experiments, IC50 was calculated by plotting x-y and fitting the data with a straight line (linear regression). The IC50 value is then estimated using the fitted line (Rekha & Anila, 2019), i.e.: Y = aX + b, IC50 = (0.5 - b)/a

DNA cleavage activity

After taking blood from the volunteer centrifugation at 1500 x g for 20 minutes, pelleted PBMCs. The nuclei-containing pellets were dispersed in 0.1 ml TE buffer (100 mM Tris-HC1 and 1 mM EDTA, pH 8) and 1 ml proteinase K buffer (100 #g/ml proteinase K, 5 mM EDTA, and 0.5 percent sodium lauroyl sarcosinate (sarkosyl), pH 8) was added to both calf thymus DNA samples and resuspended nuclei. After that, the tubes were incubated for 2 hours at 50°C. An identical volume of phenol was used to extract DNA. Then, DNA was extracted using phenol, chloroform, and isoamyl alcohol (25:24:1 v/v/v) and 2 chloroform: isoamyl alcohol (24:1 v/v). The nucleic acids were precipitated by adding ethanol (2.5 volumes) and 0.3 M sodium acetate (0.1 volumes) to the mixture and storing it at -20°C for at least 3 hours. Centrifugation was used to pellet the DNA and RNA, which were then dried under nitrogen. The pellet was dissolved in 1 ml RNase A buffer (RNase 100 mg/ml, 50 mM Tris-HCl, 10 mM EDTA, and 10 mM NaCl pH 8) and incubated for 2 hours at 37°C (this stage was omitted for calf thymus DNA). Before air drying, DNA was extracted using phenol-chloroform isoamyl alcohol, then chloroform isoamyl alcohol (x 2), and finally precipitated with ethanol and sodium acetate as before {Maixner, 2021 #1754}. Using isolated genomic DNA from PBMCs as a target, agarose gel electrophoresis was used to assess the DNA cleavage of naked Fe_3O_4 NPs, curcumin, and Fe_3O_4@CUR. The target DNA was combined with two repeats of three types of treatments (100 mM) (1: 1). The mixture was then incubated for two hours at 37 °C. The DNA and chemical mixtures were placed into wells after incubation, and the electrophoresis procedure began at a voltage of 100 V for 20 minutes. As a control, untreated genomic DNA was employed (Mousavi-Khattat, Keyhanfar, & Razmjou, 2018).

In vivo anticancer test:

All animal tests were conducted after receiving the ethical committee confirmation with the moral approval code: IR.IUMS.REC.1400.883. Mice and cancer cell line modeling experiments were performed on 6 to 8-week-old BALB / C mice weighing 20-18 g. All mice were fed in a standard laboratory. Breast tumor model, 4 T1 cell lines used for administration. The cells were cultured in RPMI medium with 10% FBS and 1% antibiotics and incubated at 37 °C with 5% CO2. One million cells in the form of subcutaneous were injected to the right of each mouse. Tumor size was determined with a caliper using the standard formula (length × width 2/2). The experiment was performed in 8 groups of BALB / C mice (3 mice in each group) aged about 35 to 40 days and weighing 20 to 22 grams. Mice were divided into two main groups (with and without tumor tissue). Therefore, in addition to each study group in which the tumor developed, a group of healthy mice was participated. The study mice were divided into the following groups: a) MNP@ CUR, b) MNPs alone, c) curcumin alone, and d) PBS. Each mouse was injected 200 µg/kg of the items mentioned intraperitoneally four times a week. Mice with tumor were weighed every four days, and their tumor sizes were measured. The mice that received the drug system (MNP@ CUR) were imaged by 3 Tesla Siemens MRI instruments in the center one week, two weeks, and three weeks apart. National Brain Mapping was performed at the University of Tehran. All treatments and principles of working with animals were performed according to the instructions of care and working with laboratory animals, which the Animal Ethics Committee approved of Iran University of Medical Sciences. (Council, 2010). The statistical analysis was done using Duncan's test (*p<0.05).

Result and Discussions

Characterization of synthesized nanoparticles

Curcumin is a highly pleiotropic molecule that interacts physically with its diverse range of molecular targets including Fe_3O_4 (Hassanzadeh-Afruzi, Dogari, Esmailzadeh, & Maleki, 2021). FTIR was used to characterize the MNPs further to verify the chemical bonds. FTIR spectra of MNPs is shown in Fig. 1. Two absorption bands below 1000 cm^{-1} in this range are known as a standard feature in all ferrites. Although this range is not unique to these compounds, spinel occurs in the spectrum of most metal oxides related to their

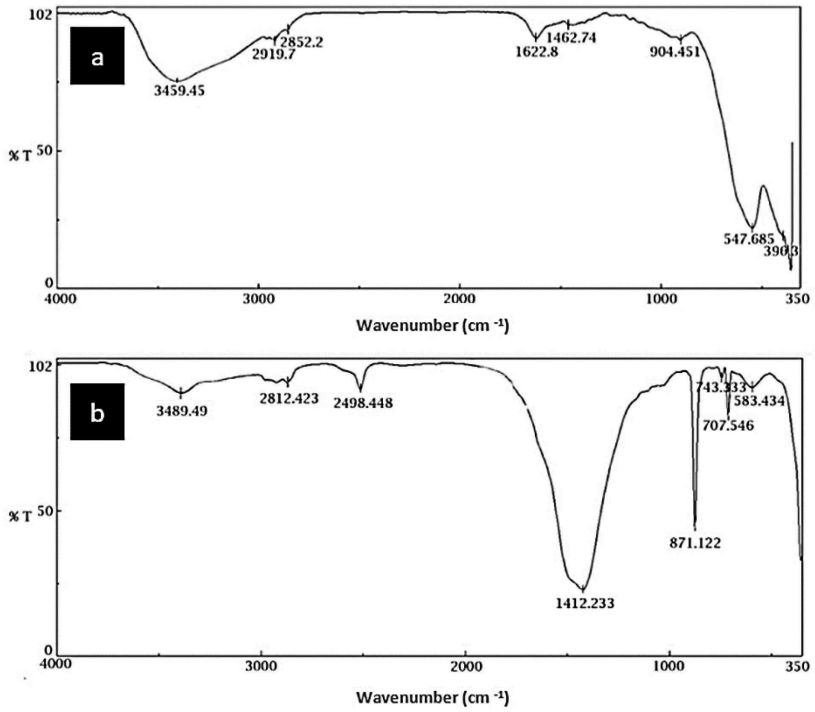

Figure 1. FTIR spectra of naked MNP **(a)** and MNP@CUR **(b)**.

vibrational states, thus confirming the presence of metal oxides (400 and 600 cm^{-1})(Jayachandran, T R, & Nair, 2021). The vibration of the Fe–O bonds in the crystalline lattice of Fe_3O_4 MNPs corresponds to the band at 580 cm^{-1} in all spectra (Hassanzadeh-Afruzi et al., 2021). In an aqueous environment, the surfaces of MNPs were rapidly covered with hydroxyl groups during chemical co-precipitation, and the typical bands of hydroxyl groups, 1630 and 3405 cm^{-1}, shown in the FTIR spectrum (Fig. 1) (Dabagh, Chaudhary, Haris, Haider, & Ali, 2018). A broad peak at 3420 cm^{-1} is related to the–OH groups of curcumin. The peaks at 1690 cm^{-1} and 1396 cm^{-1} can be assigned to the C=C and C=O vibrations in the structure of curcumin (Mehdinia, Mirzaeipour, & Jabbari, 2019).

Fig. 2 presents the XRD patterns with Gaussian fit of the peak (311) (inset) of the synthesized MNPs using the chemical co-precipitation method. In the sample, there were six distinct peaks for MNPs corresponding to (220), (311), (400), (422), (511), and (440). The position and relative intensity of all diffraction peaks match well with those of the magnetite (Asab, Zereffa, & Abdo Seghne, 2020). Even after curcumin was loaded onto the MNPs, the crystalline character was preserved.

The FESEM images of the MNP@CUR, clearly show the presence of spherical shape of MNPs with an average size of ~41 nm, which conforms with the ImageJ analysis (Fig. 3a). Images from microscopic examinations show that the particles formed are spherical and agglomerated to a shallow degree. During calcination, the agglomeration of the particles may have resulted in a net decrease in the solid-solid and solid–vapor interface free energy. Fe3O4 was reported to have a size of 7nm in one study, but when Fe3O4 was combined with SiO2, the size grew to 40 nm (Almaki et al., 2016), indicating that functionalization enhanced particle size. When the drug loading was finished, the size was raised. Drug delivery is always thought to be best when the size is less than 100 nm (Nasiri et al., 2020). Interestingly, larger Fe3O4 nanoparticles showed greater accumulation in tumors, thereby inducing more efficient tumor growth inhibition (Tian et al., 2022). The overview TEM images of MNPs and MNPs with curcumin are depicted in Fig. 3b, c. Both samples show agglomeration of round iron oxide nanoparticles. The spherical formation of naked MNPs with narrow size distribution and a mean diameter of 32 nm was demonstrated in the pictures (Fig. 3b and Fig. 4b). Therefore, the reduction in agglomeration can be

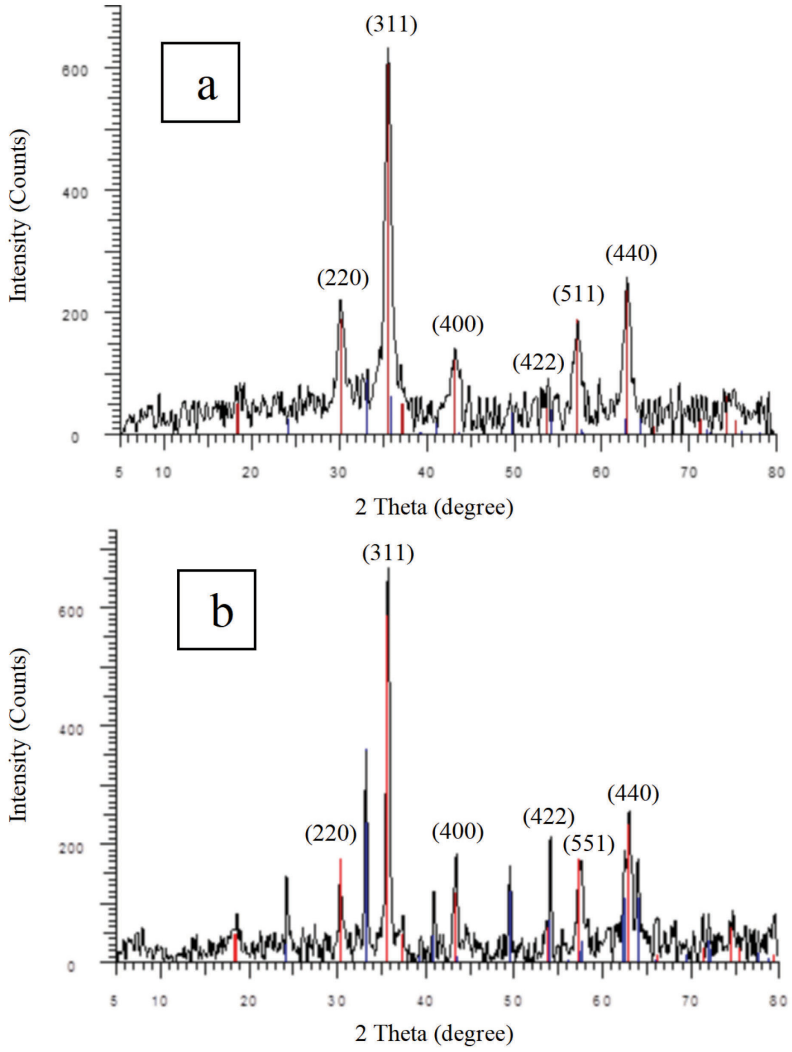

Figure 2. XRD spectra of the naked MNPs **(a)**, and MNPs@CUR **(b)**

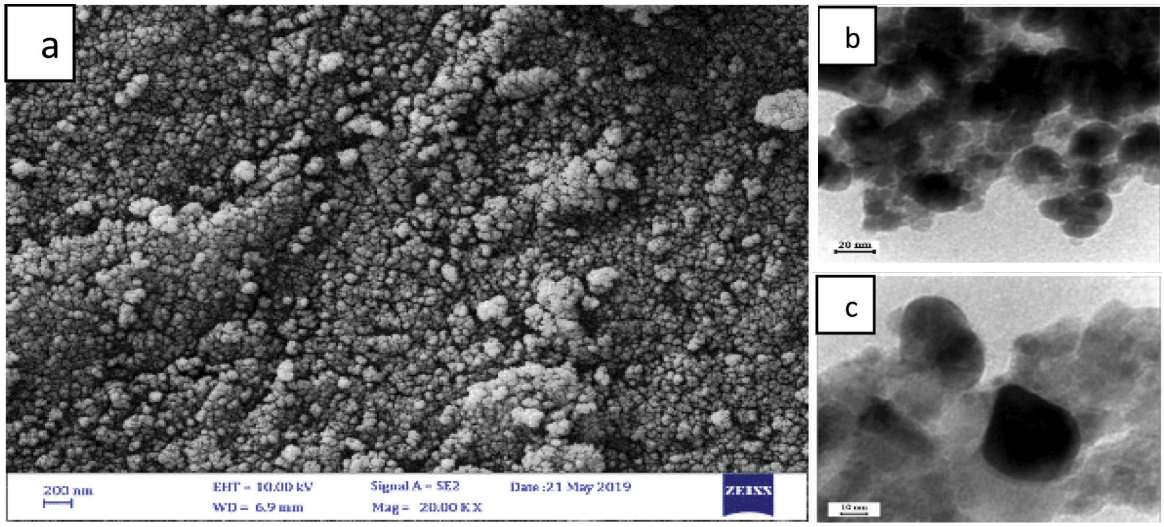

Figure 3. FE-SEM **(a)** and TEM micrographs of naked MNPs **(b)** and MNP@CUR **(c)**.

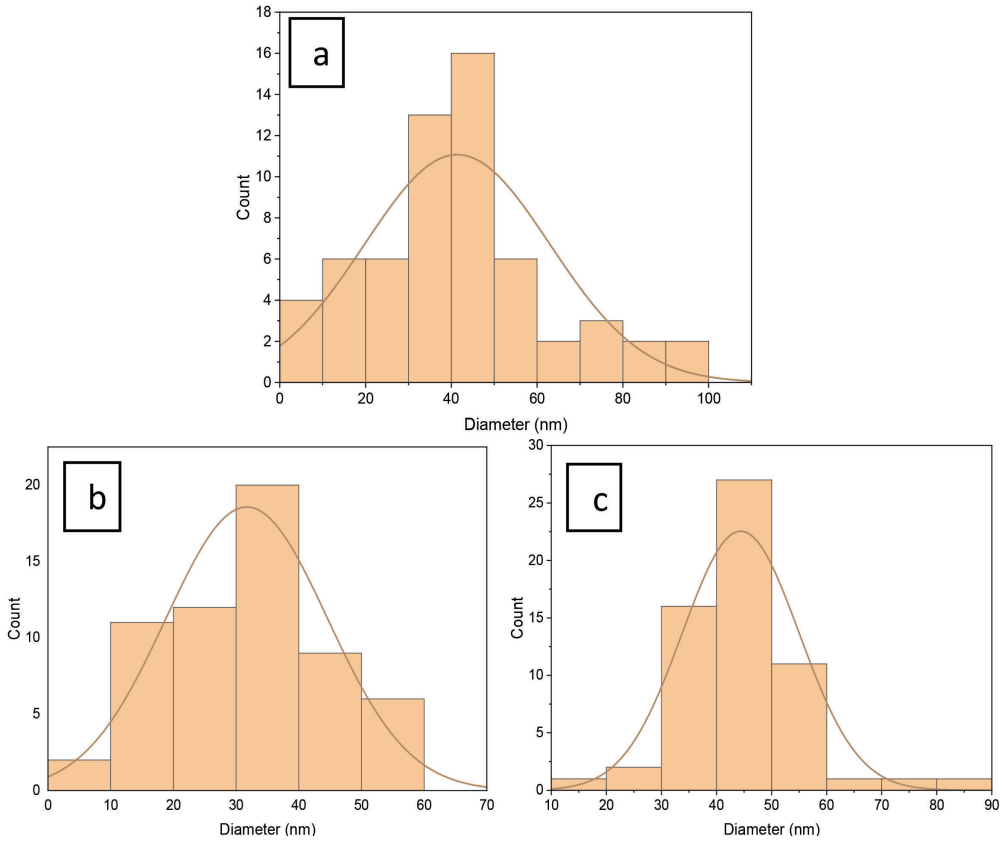

Figure 4. Size distribution of MNP@CUR acquired from SEM images **(a)**. Size distribution of naked MNP **(b)** and MNP@CUR **(c)** acquired from TEM images.

well observed. In addition, the average MNP@CUR size obtained by the SEM technique was confirmed by TEM and an average size of 44 nm was obtained through ImageJ analysis (Fig. 4c). However, several nanoparticles usually absorb each other in mass due to magnetic attraction to form the primary nucleus for the accumulation of nanoparticles. (Nasiri et al., 2020).

The magnetic property of bare MNPs and MNPs after curcumin loading were studied at room temperature (300 K) using a vibrating sample magnetometer (VSM), and results are shown in Fig. 5. Generally, the magnetic property of both nanoparticles displayed a superparamagnetic characteristic where no hysteresis loop was developed. The superparamagnetic of the nanoparticles is wholly attributed to Fe^{2+} content that occupies the octahedral sites of the inverse-spinel structure (Nasiri et al., 2020), which the superparamagnetic behavior was acquired due to their small size effect. In agreement with the literature, Fe_3O_4 particles below 50 nm exhibited a single magnetic domain that possessed no magnetic property after the magnetic field was removed (Almaki et al., 2016; Nasiri et al., 2020). The presented magnetization curve of bare MNPs has a saturation magnetization (Ms) of 35 emu/g and negligible coercivity and magnetic remanence. The magnetic property is related to particle size. The difference of Fe_3O_4 MNPs Ms compared to the bulk Fe_3O_4 (Ms = 84 emu=g and Hc = 500 to 800 Oe) owes to the increase of spin canting effect and thermal fluctuation as the particle size was reduced. The Ms value shifted down to 30 emu/g after loading curcumin. so loading the medicine on MNPs doesn't have any sensible effect on the superparamagnetic behavior of MNPs (Nasiri et al., 2020).

The surface charges of MNPs have a significant impact their rheological properties determined through zeta potential analysis. In this study, the electric charges on the surface of nanoparticles become more positive after adding curcumin, similar to previously reported studies in SPION coatings (Galli et al., 2017).

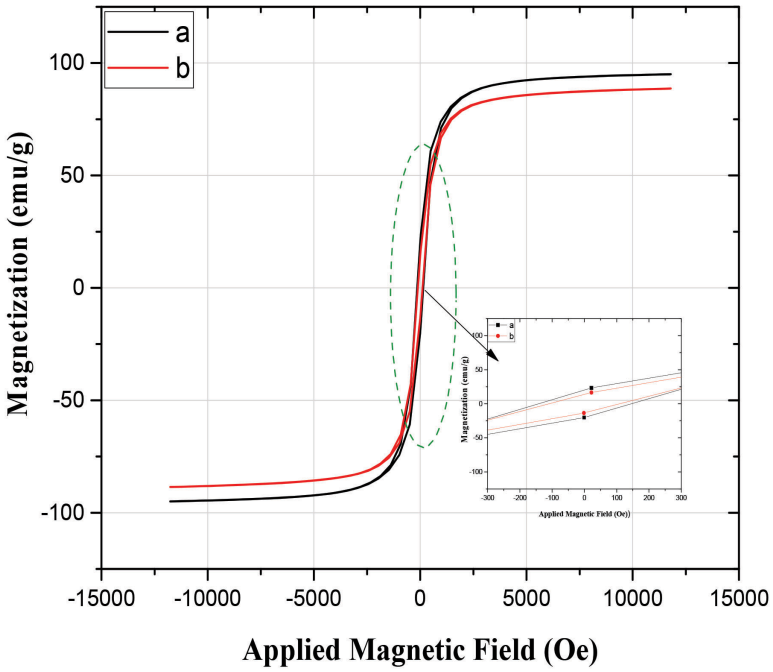

Figure 5. The magnetization curve at room temperature (300 K) of naked MNPs **(a)**, MNP@CUR **(b)**.

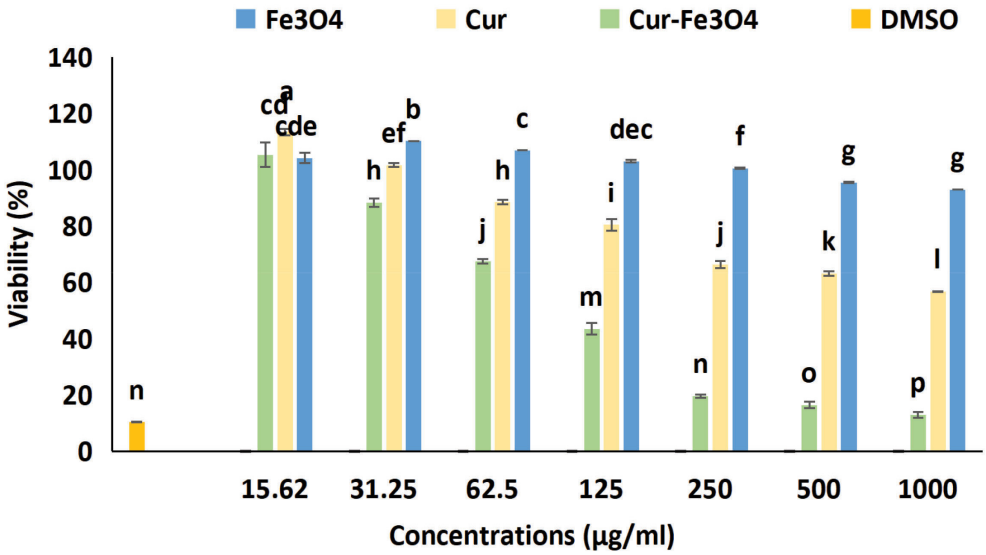

Figure 6. Percentages of 4T-1 cells treated with three groups of samples in different concentrations for 24 h. As stated by Duncan's test, different letters imply significant differences in mean values for each parameter. ($P < 0.05$).

In vitro anticancer activity

In vitro anti-cancer activity of MNPs evaluated on 4t1cell line in different concentrations. The results are shown in Fig. 6. The cancer cell death increased with increasing concentrations of both curcumin (IC50 = More than 1000 µg/ml) and curcumin-loaded MNPs (IC50=108 µg/ml). However, a negligible inhibition of cell growth was observed due to the increased naked MNPs. Microscopic images resulted in treatment with different concentrations of MNP@CUR naked MNPs, and alone curcumin, demonstrated in Fig. 7.

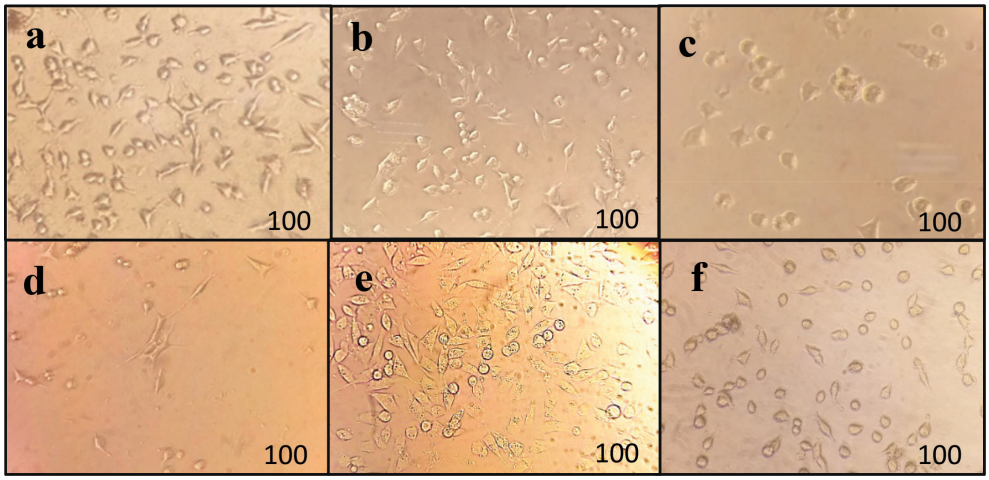

Figure 7. microscopic images of 4T-1 cells density after treatment with MNP@CUR in different concentrations (**a:** 15.62 µg/ml, **b:** 62.5 µg/ml, **c:** 250 µg/ml, **d:** 1000 µg/ml), **e:** Naked MNPs (1000 µg/ml)

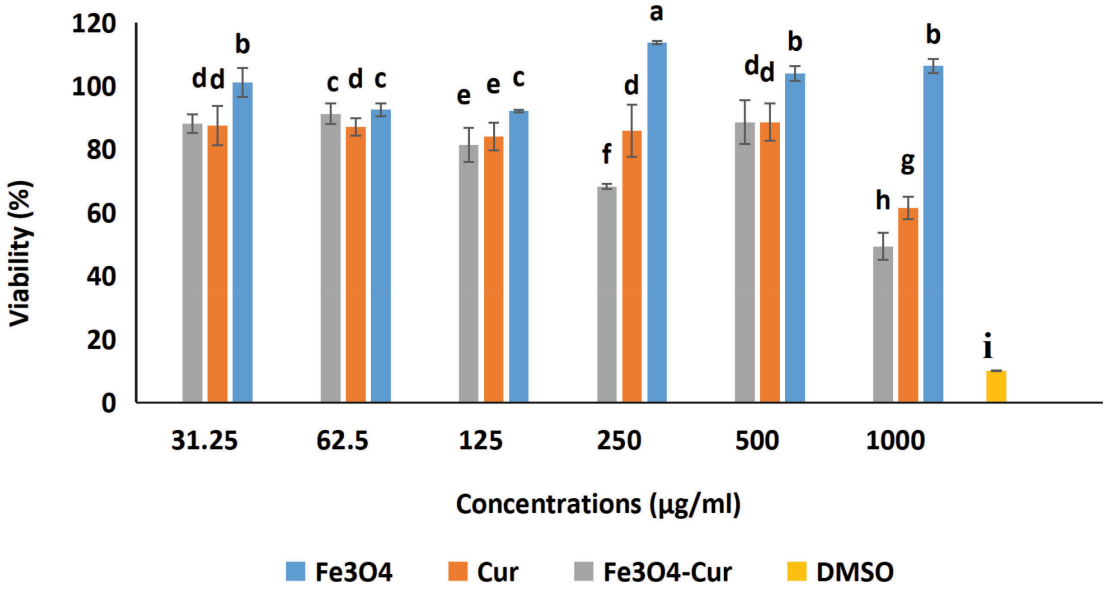

Figure 8. Percentages of normal peripheral blood mononuclear cells (PBMC) treated with three groups of samples in different concentrations for 24 h. As stated by Duncan's test, different letters imply significant differences in mean values for each parameter. ($P < 0.05$).

MNPs cytotoxicity against normal cell line

The cytotoxicity potential of the synthesized magnetic nanoparticles was tested against normal peripheral blood mononuclear cells (PBMC). This type of cell is used because chemotherapy is usually given by injecting a drug into the bloodstream. The immune response by this group of cells is greater than when whole blood is used (Betsou, Gaignaux, Ammerlaan, Norris, & Stone, 2019). The results are shown in Fig. 8. Approximately no toxicity was observed in the case of naked MNPs. However, Curcumin and MNP@CUR showed toxicities just at high concentrations. IC50 was determined to be 991 µg/ml in the case of curcumin-loaded MNP s.

DNA cleavage activity

To comprise the DNA digestion activity of curcumin, naked MNPs and MNP @CUR, DNA molecules of PBMCs were extracted, treated with the samples

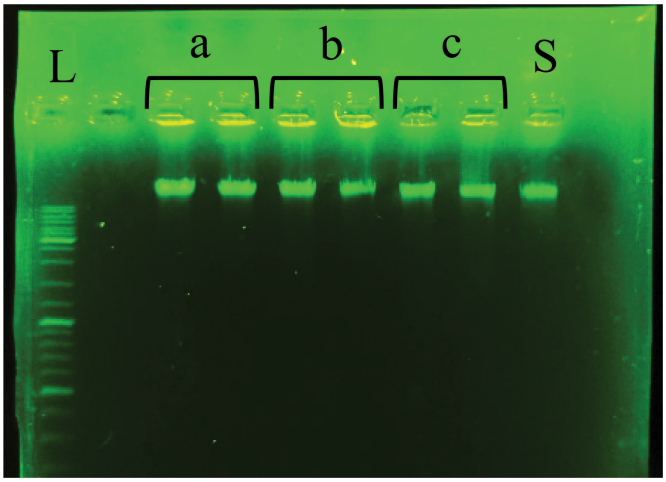

Figure 9. DNA cleavage activities of MNP@CUR (a: repeated two times), curcumin (b: repeated two times) and naked magnetic nanoparticles (c: repeated two times). The control DNA without any treatment was shown at lane S. Lane "L" loaded with DNA ladder.

and analyzed through the Gel electrophoresis method (Fig. 9). No digestion activity was shown against DNA for three treatments in comparison with the control band related to untreated genomic DNA demonstrating the magnetic drug delivery system synthesized in this study is not toxic against the DNA of normal cells.

In vivo anticancer test

Using cell line 4t1, breast cancer tumors were created in mice. This experiment was conducted to evaluate the anti-cancer effects of curcumin, and magnetic nanoparticles coated with curcumin. In this experiment, phosphate buffer was used as a control sample. In this study, in addition to the four groups of mice that were selected for treatment with four samples, four other groups of mice were considered as negative controls with no treatment to ensure that the environment does not affect the death of mice. At the end of the test, the mice that were not treated were all healthy and alive. The results of the test and measuring the diameter of the tumors showed that the mice that were treated with curcumin and nanoparticles coated with it had tumors with a smaller diameter, while the mice that were treated with uncoated nanoparticles and phosphate buffer did not have a decrease in the size of their tumors (Fig. 10). Nanoparticles coated with curcumin significantly inhibited tumor growth. As shown in Fig. 11, mice receiving curcumin-loaded nanoparticles were associated with a reduction in tumor size after 7 days, and after 14 days, the tumor almost wholly disappeared. The size of the tumors of the mice treated with curcumin alone also decreased significantly...

Discussion

Some scientists have successfully studied anti-tumor magnetic drug carriers and their effects on laboratory animals. (Ak, Yilmaz, Güneş, Hamarat Sanlier, & biotechnology, 2018). In this paper, a comprehensive study was performed on the cytotoxicity effect of curcumin-loaded drug delivery system on cancer and normal cell lines through *In vitro* and *In vivo* studies. The results of physicochemical characterizations such as size, charge, surface morphology and FTIR spectroscopy indicated the accuracy of curcumin-loaded nanoparticle synthesis. *In vitro* and *In vivo* studies were performed to evaluate the efficacy of nanoparticles as carriers of the drug. Based on *In vitro* studies, the cytotoxic effect of curcumin and nanoparticles loaded with curcumin had a time and dose-dependent behavior. In addition, studies have shown an increased *In vitro* anti-proliferative effect of curcumin-loaded nanoparticles compared to free drug on the 4t1cell line. This could be due to the increased permeability of curcumin as an anticancer agent when coated on nanoparticles. As can be seen in the results, the nanoparticles alone showed almost no anti-cancer effect, contrary to curcumin. Also, after performing a cytotoxicity test on peripheral blood lymphocytes, it was found that

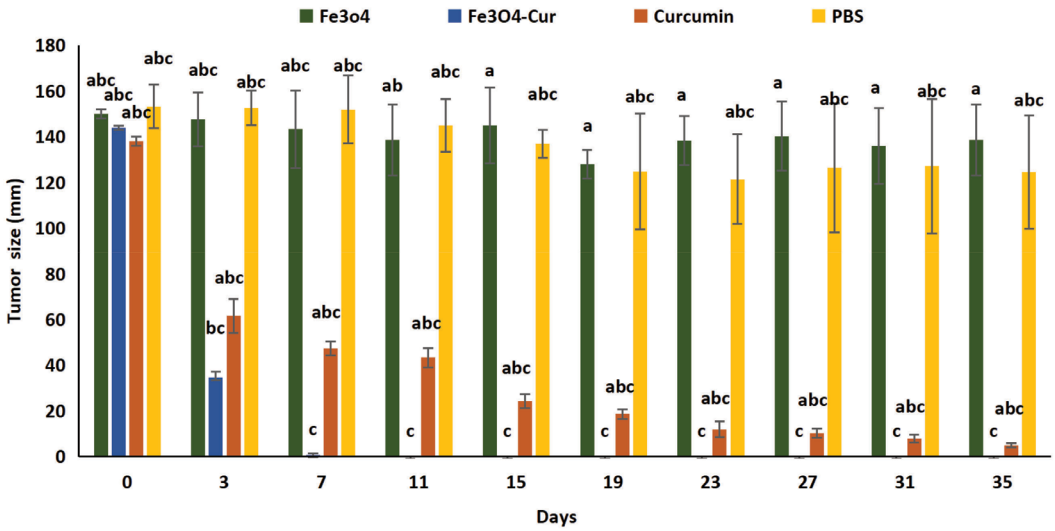

Figure 10. Tumor diameter of four groups (control (PBS), curcumin, naked and curcumin coated nanoparticles treatment up to 35 days with a time interval of 4 days measuring. As stated by Duncan's test, different letters imply significant differences in mean values for each parameter ($P < 0.05$).

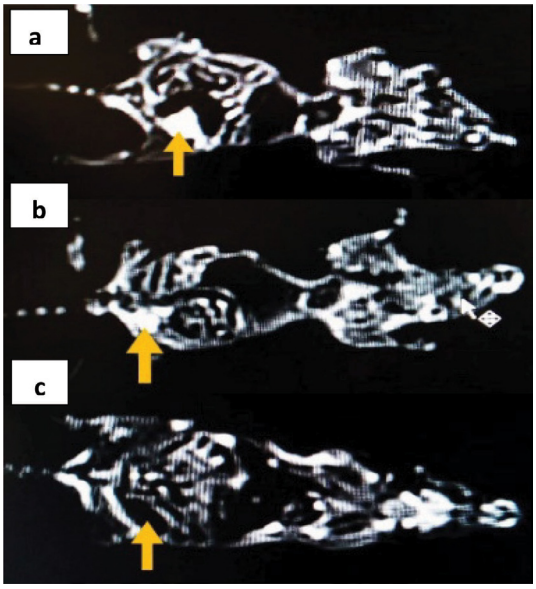

Figure 11. Anti-proliferative effect of Fe3O4@CUR on the transplantable tumors. a: MRI Photograph showing mice without no treatment after two weeks. b: MRI Photograph of the mice treated with MNP-CUR after 7 days. c: MRI Photograph of the mice treated with MNP-CUR after 14 days' volume was measured once every 4 days.

magnetic nanoparticles, curcumin and curcumin-coated magnetic nanoparticles showed almost no toxicity except in high concentrations. The IC50 of 108 µg/ml for anticancer effect and IC50 of 991 µg/ml for toxicity effect against normal cells in the case of curcumin-coated magnetic nanoparticles indicates the low toxicity of the synthesized drug system for regular and non-cancerous cells of animals meanwhile high toxicity against cancerous cells. Cytotoxicity of drug delivery systems against normal body cells such as mononuclear blood cells is significant. A challenge that has been given a lot of attention in this article compared to previous articles (B. Dutta et al., 2022; Nguyen, Luong, Pham, Tran, & Dang, 2022). so that these systems are not toxic against normal body cells and can act as drugs with very low side effects, after studying the impact of treatments on DNA and its digestibility, it was found that curcumin magnetic nanoparticles and curcumin-coated magnetic nanoparticles do not show significant DNA digestion activity. The results indicate more safety of the drug system for use in cellular environments than other previously reported nanoparticles through which DNA is destroyed to a great extent (Mousavi-Khattat et al., 2018). Also, the *in vivo* results are similar to those seen in *In vitro* studies and show that the efficiency of the drug system of curcumin-coated magnetic nanoparticles is much higher than that of curcumin alone and has been able to remove tumors in mice within a week. In contrast, Curcumin alone, after 35 days, still leaves some tumor in the mice.

Conclusion

Drug delivery systems, especially magnetic nanoparticles, have been proposed as a new

research field in nanotechnology. This study developed magnetic iron nanoparticles coated by anticancer phytochemical curcumin as an efficient drug delivery system. Due to the high aspect ratio and penetration ability of the nanoparticles, the enhancement of the anticancer effect of the curcumin was demonstrated. Furthermore, cytotoxicity and genotoxicity analysis of the coated particles against normal cells showed that the drug delivery system has no significant toxicity and could provide safe conditions for use in the biological space of the body. Based on the results of this study, it seems that curcumin-loaded magnetic nanoparticles can be introduced as an effective drug carrier in the chemotherapy process to improve breast cancer and reduce drug side effects.

Acknowledgement

We want to thank the "SET-UP" laboratory members at Isfahan Science and Technology Town (ISTT), Isfahan University of Technology, Isfahan, Iran, for accompanying us to accomplish the project.

Conflict of Interest

The authors declare no competing interests.

References

Abdallah, F. M., Helmy, M. W., Katary, M. A., & Ghoneim, A. I. J. N.-S. s. a. o. p. (2018). Synergistic antiproliferative effects of curcumin and celecoxib in hepatocellular carcinoma HepG2 cells. *391*(12), 1399-1410.

Abotaleb, M., Kubatka, P., Caprnda, M., Varghese, E., Zolakova, B., Zubor, P., . . . Pharmacotherapy. (2018). Chemotherapeutic agents for the treatment of metastatic breast cancer: An update. *101*, 458-477.

Aguilera, G., Berry, C. C., West, R. M., Gonzalez-Monterrubio, E., Angulo-Molina, A., Arias-Carrión, Ó., & Méndez-Rojas, M. Á. J. N. A. (2019). Carboxymethyl cellulose coated magnetic nanoparticles transport across a human lung microvascular endothelial cell model of the blood–brain barrier. *1*(2), 671-685.

Ak, G., Yilmaz, H., Güneş, A., Hamarat Sanlier, S. J. A. c., nanomedicine,, & biotechnology. (2018). *In vitro* and *in vivo* evaluation of folate receptor-targeted a novel magnetic drug delivery system for ovarian cancer therapy. *46*(sup1), 926-937.

Ali, M., & Smiley, R. J. T. F. J. (2018). Curcumin Induces Apoptosis via the Capase-8 Activated Extrinsic Pathway in MDA-MB-231 Breast Cancer Cells. *32*, 664.666-664.666.

Almaki, J. H., Nasiri, R., Idris, A., Majid, F. A. A., Salouti, M., Wong, T. S., . . . Amini, N. (2016). Synthesis, characterization and *in vitro* evaluation of exquisite targeting SPIONs–PEG–HER in HER2+ human breast cancer cells. *Nanotechnology, 27*(10), 105601.

Arsalani, S., Guidelli, E. J., Silveira, M. A., Salmon, C. E., Araujo, J. F., Bruno, A. C., . . . Materials, M. (2019). Magnetic Fe3O4 nanoparticles coated by natural rubber latex as MRI contrast agent. *475*, 458-464.

Asab, G., Zereffa, E. A., & Abdo Seghne, T. J. I. j. o. b. (2020). Synthesis of silica-coated Fe3O4 nanoparticles by microemulsion method: characterization and evaluation of antimicrobial activity. *2020*.

Bai, Y., An, N., Chen, D., Liu, Y.-z., Liu, C.-p., Yao, H., . . . Tian, W. J. C. P. (2020). Facile construction of shape-regulated β-cyclodextrin-based supramolecular self-assemblies for drug delivery. *231*, 115714.

Baki, A., Remmo, A., Löwa, N., Wiekhorst, F., & Bleul, R. J. I. J. o. M. S. (2021). Albumin-coated single-core iron oxide nanoparticles for enhanced molecular magnetic imaging (Mri/mpi). *22*(12), 6235.

Bakshi, S., Zakharchenko, A., Minko, S., Kolpashchikov, D. M., & Katz, E. J. M. (2019). Towards nanomaterials for cancer theranostics: a system of DNA-modified magnetic nanoparticles for detection and suppression of RNA marker in cancer cells. *5*(2), 24.

Betsou, F., Gaignaux, A., Ammerlaan, W., Norris, P. J., & Stone, M. (2019). Biospecimen Science of Blood for Peripheral Blood Mononuclear Cell (PBMC) Functional Applications. *Current Pathobiology Reports, 7*(2), 17-27. doi:10.1007/s40139-019-00192-8

Brenner, D. R., Weir, H. K., Demers, A. A., Ellison, L. F., Louzado, C., Shaw, A., . . . Smith, L. M. J. C. (2020). Projected

estimates of cancer in Canada in 2020. *192*(9), E199-E205.

Bu, L. L., Rao, L., Yu, G. T., Chen, L., Deng, W. W., Liu, J. F., . . . Zhao, X. Z. J. A. F. M. (2019). Cancer stem cell-platelet hybrid membrane-coated magnetic nanoparticles for enhanced photothermal therapy of head and neck squamous cell carcinoma. *29*(10), 1807733.

Chenthamara, D., Subramaniam, S., Ramakrishnan, S. G., Krishnaswamy, S., Essa, M. M., Lin, F.-H., & Qoronfleh, M. W. (2019). Therapeutic efficacy of nanoparticles and routes of administration. *Biomaterials Research, 23*(1), 20. doi:10.1186/s40824-019-0166-x

Cianfruglia, L., Minnelli, C., Laudadio, E., Scirè, A., & Armeni, T. J. A. (2019). Side effects of curcumin: Epigenetic and antiproliferative implications for normal dermal fibroblast and breast cancer cells. *8*(9), 382.

Council, N. R. (2010). Guide for the care and use of laboratory animals.

D'Angelo, N. A., Noronha, M. A., Kurnik, I. S., Câmara, M. C., Vieira, J. M., Abrunhosa, L., . . . Ataide, J. A. J. I. J. o. P. (2021). Curcumin encapsulation in nanostructures for cancer therapy: A 10-year overview. *604*, 120534.

Dabagh, S., Chaudhary, K., Haris, S. A., Haider, Z., & Ali, J. (2018). Aluminium Substituted Ferrite Nanoparticles with Enhanced Antibacterial Activity. *Journal of Computational and Theoretical Nanoscience, 15*(3), 1052-1058.

Desreux, J. A. J. E. j. o. o., gynecology, & biology, r. (2018). Breast cancer screening in young women. *230*, 208-211.

Dutta, B., Shelar, S. B., Rajan, V., Checker, S., Divya, Barick, K. C., . . . Hassan, P. A. (2022). Gelatin grafted Fe3O4 based curcumin nanoformulation for cancer therapy. *Journal of Drug Delivery Science and Technology, 67*, 102974. doi: https://doi.org/10.1016/j.jddst.2021.102974

Dutta, P., Sarkissyan, M., Paico, K., Wu, Y., Vadgama, J. V. J. B. c. r., & treatment. (2018). MCP-1 is overexpressed in triple-negative breast cancers and drives cancer invasiveness and metastasis. *170*(3), 477-486.

Finnegan, M. T. V., Herbert, K. E., Evans, M. D., Griffiths, H. R., & Lunec, J. (1996). Evidence for sensitisation of DNA to oxidative damage during isolation. *Free Radical Biology and Medicine, 20*(1), 93-98. doi: https://doi.org/10.1016/0891-5849(95)02003-9

Fratantonio, D., Molonia, M. S., Bashllari, R., Muscarà, C., Ferlazzo, G., Costa, G., . . . Speciale, A. J. P. (2019). Curcumin potentiates the antitumor activity of Paclitaxel in rat glioma C6 cells. *55*, 23-30.

Fu, S., Li, G., Zang, W., Zhou, X., Shi, K., & Zhai, Y. J. A. P. S. B. (2021). Pure drug nano-assemblies: A facile carrier-free nanoplatform for efficient cancer therapy.

Galli, M., Guerrini, A., Cauteruccio, S., Thakare, P., Dova, D., Orsini, F., . . . Licandro, E. (2017). Superparamagnetic iron oxide nanoparticles functionalized by peptide nucleic acids. *RSC Adv., 7*, 15500-15512. doi:10.1039/C7RA00519A

George Kallivalappil, G., & Kuttan, G. J. I. (2019). Efficacy of punarnavine in restraining organ-specific tumour progression in 4T1-induced murine breast tumour model. *27*(4), 701-712.

Gómez-Archila, L. G., Palomino-Schätzlein, M., Zapata-Builes, W., & Galeano, E. J. P. o. (2021). Development of an optimized method for processing peripheral blood mononuclear cells for 1H-nuclear magnetic resonance-based metabolomic profiling. *16*(2), e0247668.

Guney Eskiler, G., Sahin, E., Deveci Ozkan, A., Cilingir Kaya, O. T., Kaleli, S. J. N., & Cancer. (2020). Curcumin induces DNA damage by mediating homologous recombination mechanism in triple negative breast cancer. *72*(6), 1057-1066.

Hassanzadeh-Afruzi, F., Dogari, H., Esmailzadeh, F., & Maleki, A. (2021). Magnetized melamine-modified polyacrylonitrile (PAN@melamine/Fe3O4) organometallic nanomaterial: Preparation, characterization, and application as a multifunctional catalyst in the synthesis of bioactive dihydropyrano [2,3-c] pyrazole and 2-amino-3-cyano 4H-pyran derivatives. *35*(10), e6363. doi: https://doi.org/10.1002/aoc.6363

Hwang, J.-h., Jeong, H., Jung, Y.-o., Nam, K. T., & Lim, K.-M. (2021). Skin irritation and inhalation toxicity of biocides evaluated with reconstructed human epidermis

and airway models. *Food and Chemical Toxicology, 150*, 112064. doi: https://doi.org/10.1016/j.fct.2021.112064

Jayachandran, A., T R, A., & Nair, A. (2021). Green synthesis and characterization of zinc oxide nanoparticles using Cayratia pedata leaf extract. *Biochemistry and Biophysics Reports, 26*, 100995. doi:10.1016/j.bbrep.2021.100995

Justin, C., Samrot, A. V., Sahithya, C. S., Bhavya, K. S., & Saipriya, C. J. P. O. (2018). Preparation, characterization and utilization of coreshell super paramagnetic iron oxide nanoparticles for curcumin delivery. *13*(7), e0200440.

Khan, A. Q., Ahmed, E. I., Elareer, N., Fathima, H., Prabhu, K. S., Siveen, K. S., . . . Ahmad, A. J. I. j. o. m. s. (2020). Curcumin-mediated apoptotic cell death in papillary thyroid cancer and cancer stem-like cells through targeting of the JAK/STAT3 signaling pathway. *21*(2), 438.

Lee, W.-H., Loo, C.-Y., Rohanizadeh, R. J. M. S., & C, E. (2019). Functionalizing the surface of hydroxyapatite drug carrier with carboxylic acid groups to modulate the loading and release of curcumin nanoparticles. *99*, 929-939.

Lopez-Barbosa, N., Suárez-Arnedo, A., Cifuentes, J., Gonzalez Barrios, A. F., Silvera Batista, C. A., Osma, J. F., . . . Engineering. (2019). Magnetite–OmpA Nanobioconjugates as Cell-Penetrating Vehicles with Endosomal Escape Abilities. *6*(1), 415-424.

Mehdinia, A., Mirzaeipour, R., & Jabbari, A. (2019). Nanosized Fe3O4–curcumin conjugates for adsorption of heavy metals from seawater samples. *Journal of the Iranian Chemical Society, 16*(7), 1431-1439. doi:10.1007/s13738-019-01619-0

Mousavi-Khattat, M., Keyhanfar, M., & Razmjou, A. (2018). A comparative study of stability, antioxidant, DNA cleavage and antibacterial activities of green and chemically synthesized silver nanoparticles. *Artif Cells Nanomed Biotechnol, 46*(sup3), S1022-s1031. doi:10.1080/21691401.2018.1527346

Nam, K. C., Han, Y. S., Lee, J.-M., Kim, S. C., Cho, G., & Park, B. J. J. C. (2020). Photo-functionalized magnetic nanoparticles as a nanocarrier of photodynamic anticancer agent for biomedical theragnostics. *12*(3), 571.

Nasiri, R., Dabagh, S., Meamar, R., Idris, A., Muhammad, I., Irfan, M., & Nodeh, H. R. (2020). Papain grafted into the silica coated iron-based magnetic nanoparticles 'IONPs@ SiO2-PPN'as a new delivery vehicle to the HeLa cells. *Nanotechnology, 31*(19), 195603.

Nguyen, N. Y., Luong, H. V. T., Pham, D. T., Tran, T. B. Q., & Dang, H. G. (2022). Chitosan-functionalized Fe3O4@SiO2 nanoparticles as a potential drug delivery system. *Chemical Papers, 76*(7), 4561-4570. doi:10.1007/s11696-022-02189-x

Nigjeh, S. E., Yeap, S. K., Nordin, N., Rahman, H., & Rosli, R. J. M. (2019). *In vivo* anti-tumor effects of citral on 4T1 breast cancer cells via induction of apoptosis and downregulation of aldehyde dehydrogenase activity. *24*(18), 3241.

Nosrati, H., Salehiabar, M., Attari, E., Davaran, S., Danafar, H., & Manjili, H. K. J. A. O. C. (2018). Green and one-pot surface coating of iron oxide magnetic nanoparticles with natural amino acids and biocompatibility investigation. *32*(2), e4069.

O'Meara, T., Marczyk, M., Qing, T., Yaghoobi, V., Blenman, K., Cole, K., . . . Pusztai, L. J. J. P. O. (2020). Immunological differences between immune-rich estrogen receptor–positive and immune-rich triple-negative breast cancers. *3*, 767-779.

Oroujeni, M., Kaboudin, B., Xia, W., Jönsson, P., & Ossipov, D. A. J. P. i. O. C. (2018). Conjugation of cyclodextrin to magnetic Fe3O4 nanoparticles via polydopamine coating for drug delivery. *114*, 154-161.

Osorio Jaimes, M. J. (2020). Produced water demulsification using maghemite nanoparticles.

Ostroverkhov, P., Semkina, A., Naumenko, V., Plotnikova, E., Melnikov, P., Abakumova, T., . . . science, i. (2019). Synthesis and characterization of bacteriochlorin loaded magnetic nanoparticles (MNP) for personalized MRI guided photosensitizers delivery to tumor. *537*, 132-141.

Palesh, O., Scheiber, C., Kesler, S., Mustian, K., Koopman, C., & Schapira, L. J. T. b. j. (2018). Management of side effects during and post-treatment in breast cancer survivors. *24*(2), 167-175.

Pan, R., Zeng, Y., Liu, G., Wei, Y., Xu, Y., & Tao, L. J. P. C. (2020). Curcumin–polymer

conjugates with dynamic boronic acid ester linkages for selective killing of cancer cells. *11*(7), 1321-1326.

Patra, S., Pradhan, B., Nayak, R., Behera, C., Rout, L., Jena, M., . . . Bhutia, S. K. (2021). *Chemotherapeutic efficacy of curcumin and resveratrol against cancer: Chemoprevention, chemoprotection, drug synergism and clinical pharmacokinetics.* Paper presented at the Seminars in cancer biology.

Rekha, S., & Anila, E. J. M. L. (2019). *In vitro* cytotoxicity studies of surface modified CaS nanoparticles on L929 cell lines using MTT assay. *236*, 637-639.

Roychoudhury, S., Chakraborty, S., Das, A., Guha, P., Agarwal, A., & Henkel, R. (2021). Herbal medicine use to treat andrological problems: Asian and Indian subcontinent: Ginkgo biloba, Curcuma longa, and Camellia sinensis. In (pp. 129-146).

Septisetyani, E., Santoso, A., Wisnuwardhani, P., & Prasetyaningrum, P. (2020). *Cytotoxic effects of chemopreventive agents curcumin, naringin and epigallocathecin-3-gallate in C2C12 myoblast cells*. Paper presented at the IOP Conference Series: Earth and Environmental Science.

Shah, M., Murad, W., Mubin, S., Ullah, O., Rehman, N. U., & Rahman, M. H. (2022). Multiple health benefits of curcumin and its therapeutic potential. *Environmental Science and Pollution Research, 29*(29), 43732-43744. doi:10.1007/s11356-022-20137-w

Sun, H., Zhang, B., Jiang, X., Liu, H., Deng, S., Li, Z., & Shi, H. J. N. (2019). Radiolabeled ultra-small Fe3O4 nanoprobes for tumor-targeted multimodal imaging. *14*(1), 5-17.

Sung, H., Ferlay, J., Siegel, R. L., Laversanne, M., Soerjomataram, I., Jemal, A., & Bray, F. (2021). Global Cancer Statistics 2020: GLOBOCAN Estimates of Incidence and Mortality Worldwide for 36 Cancers in 185 Countries. *71*(3), 209-249. doi: https://doi.org/10.3322/caac.21660

Tian, X., Ruan, L., Zhou, S., Wu, L., Cao, J., Qi, X., . . . Shen, S. (2022). Appropriate Size of Fe3O4 Nanoparticles for Cancer Therapy by Ferroptosis. *ACS Applied Bio Materials, 5*(4), 1692-1699. doi:10.1021/acsabm.2c00068

Wang, D., Zhu, K., Tian, J., Li, Z., Du, G., Guo, Q., . . . Biology. (2018). Clinicopathological and ultrasonic features of triple-negative breast cancers: a comparison with hormone receptor-positive/human epidermal growth factor receptor-2-negative breast cancers. *44*(5), 1124-1132.

Wu, L., Zong, L., Ni, H., Liu, X., Wen, W., Feng, L., . . . Shen, S. J. B. s. (2019). Magnetic thermosensitive micelles with upper critical solution temperature for NIR triggered drug release. *7*(5), 2134-2143.

Yusefi, M., Shameli, K., & Jumaat, A. F. J. J. o. A. R. i. M. S. (2020). Preparation and properties of magnetic iron oxide nanoparticles for biomedical applications: A brief review. *75*(1), 10-18.

Zoi, V., Galani, V., Vartholomatos, E., Zacharopoulou, N., Tsoumeleka, E., Gkizas, G., . . . Leonardos, I. J. B. (2021). Curcumin and Radiotherapy Exert Synergistic Anti-Glioma Effect *In Vitro*. *9*(11), 1562.